Chemically Modifiable Fluorinated Copolymer Nanoparticles for ^{19}F MRI Contrast Enhancement

Mark M. Bailey[1,2], Steven R. Kline[3], Michael D. Anderson[2,4], Jessica Staymates[2], and Cory Berkland[1,5,*]

[1]Department of Chemical & Petroleum Engineering, University of Kansas, Lawrence, KS, USA 66047
[2]National Institute of Standards and Technology, 100 Bureau Drive, Mail Stop 8371, Gaithersburg, MD, USA 20899
[3]NIST Center for Neutron Research, 100 Bureau Drive, Mail Stop 6102, Gaithersburg, MD, USA 20899
[4]Department of Chemistry, University of Oregon, Eugene, OR, USA 97403
[5]Department of Pharmaceutical Chemistry, University of Kansas, Lawrence, KS, USA 66047

[*]Corresponding Author:
Address: 2030 Becker Drive, Lawrence, KS 66047;
Telephone: 785-864-1455;
Fax: 785-864-1454;
Email: berkland@ku.edu

Keywords

Small Angle Neutron Scattering (SANS), Ultra-Small Angle Neutron Scattering (USANS), Fluorinated Polymers, ^{19}F Magnetic Resonance Imaging, Nanoparticles

Abstract

Recently there has been interest in developing imaging contrast media for magnetic resonance imaging (MRI) that contain biologically rare, magnetically active nuclei such as fluorine. In principle, fluorinated contrast agents can be used to generate highly-selective ^{19}F magnetic resonance images that can be superimposed over complimentary ^{1}H magnetic resonance images to provide an anatomical context for the fluorinated contrast agent. Additionally, nanoparticles can be made to target various pathological sites via active and passive targeting mechanisms. In this study, fluorinated nanoparticles were produced using a free radical polymerization of vinyl formamide monomers with two different fluorinated monomers. The nanoparticles showed a clear, single ^{19}F-NMR signal. Additionally, surface amide groups were hydrolyzed to primary amines to yield additional surface reactivity. Fluorinated nanoparticles produced using a free radial polymerization method yield a new nanoparticle for ^{19}F magnetic resonance imaging applications with potential for facile functionalization.

I. Introduction

Magnetic resonance imaging (MRI) is a powerful diagnostic imaging tool that is both noninvasive and nondestructive. Paramagnetic contrast agents, such as gadolinium chelates, are often used to accelerate proton relaxation and can be employed to reveal features that might otherwise be obscured as a result of similarities in the relaxation times of adjacent tissues.[1-3] Although MRI has been an effective diagnostic tool, often the contrast changes are ambiguous and difficult to interpret. Additionally, the biological impact of traditional Gd^{3+} ion chelates, particularly macromolecular agents, is poorly understood.[4] To overcome these challenges, there has been intense interest in developing contrast media containing biologically rare, magnetically active nuclei, such as fluorine.[1, 5-10] Fluorinated materials are an excellent choice for this application because of fluorine's biological rarity and magnetic properties, and because of the excellent biocompatibility demonstrated by fluorinated colloids.[11-13] In principle, the rarity in physiological fluorine can be exploited to generate highly-selective ^{19}F images that can be superimposed over complimentary ^{1}H images, providing an anatomical context for the fluorinated contrast agent.[14, 15] Additionally, developing nanoparticle-based contrast agents that have the ability to actively or passively target tissues with specific pathologies, such as tumor tissue and atherosclerotic plaques, could enable clinicians to better diagnose such conditions using MRI.

A specific example of an active targeting strategy involves conjugating nanoparticles with ligands that bind cellular antigens associated with a

pathological site of interest. Such approaches aim to amplify the accumulation of nanoparticles to the target site.[16, 17] A potential passive targeting strategy that may be specifically applicable to tumor targeting exploits the abnormalities of tumor vasculature that cause leakage of macromolecular agents and nanoparticles into the tumor interstitium. This phenomenon is known as the enhanced permeability and retention effect, or EPR effect, and can potentially be exploited by controlling the nanoparticle size.[17-21]

A novel approach to fluorinated nanoparticles was developed for biomedical imaging using ^{19}F-MRI.[17] Chemically crosslinked nanoparticles and linear polymers were synthesized by copolymerizing two different fluorinated monomers with N-vinyl formamide. Amide groups on the nanoparticles and polymers were then hydrolyzed to their corresponding amines, thus liberating reactive sites for potential modification (e.g. targeting ligands). Results suggested that these nanomaterials may be suitable for imaging using ^{19}F-MRI.

II. Experimental Section

Materials: All materials were purchased from Sigma-Aldrich (St. Louis, MO) unless otherwise stated.* 1H,H-perfluoro-n-octyl acrylate was purchased from ExFluor Research Corporation (Round Rock, TX). 2-(allyl)hexafluoroisopropanol was purchased from Matrix Scientific (Columbia, SC). Vazo-52 was purchased from DuPont (Wilmington, DE). Dialysis

* Certain commercial equipments, instruments, or materials are identified in this article to specify adequately the experimental procedure. Such identification does not imply recommendation or endorsement by the National Institute of Standards and Technology, nor does it imply that the materials or equipment identified are necessarily the best available for the purpose.

membranes were purchased from Spectrum Labs (Rancho Dominquez, CA). Prior to nanoparticle synthesis, (1,5-N-vinylformamido) ethyl ether was synthesized as previously described.[22] Impurities were precipitated out of N-vinylformamide using absolute ethanol prior to use. All other reagents were used as received.

Synthesis of Fluorinated Nanoparticles: Nanoparticles were synthesized using a free radical polymerization technique as described previously.[23] First, 20 µL of N-vinylformamide, 20 µL of (1,5-N-vinylformamido) ethyl ether, and 20 µL of the fluorinated monomer (either 1H,H-perfluoro-n-octyl acrylate, or 2-(allyl)hexafluoroisopropanol) were dissolved in absolute ethanol containing 0.015 mg/mL polyvinylpyrrolidone (PVP) as a surfactant (MW approximately 360 kDa). Next, 6.9 mg of (E)-2,2'-(diazene-1,2-diyl)bis(2,4-dimethylpentanenitrile) (Vazo-52) were added to the solution as an initiator (Figure 1). The reagent mixture was then sparged with argon for 10 minutes to remove dissolved oxygen, then heated in a silicone oil bath to 60°C and stirred at approximately 900 RPM. The reaction was carried out isothermally under an argon atmosphere for 24 hours. The product was then dialyzed against deionized water using a 1 kDa MWCO regenerated cellulose ester dialysis tube (Spectrum Laboratories, Inc., Rancho Dominquez, CA) for 24 hours. The dialysate was changed at least 5 times to ensure complete solvent exchange. Linear polymers were synthesized analogously, but without the addition of (1,5,-N-vinylformamido) ethyl ether crosslinker or PVP surfactant. Particles were then further purified by

centrifugation for 1 hour at 18,000 rpm. Each centrifugation cycle was repeated at least 3 times.

For the hydrolysis step, particle and polymer suspensions were flash-frozen in liquid nitrogen and then lyophilized. Samples were resuspended in 1 M $NaOH_{(aq)}$ and sonicated for 1 hour at ambient temperature, as described previously.[24] The pH of each solution was then titrated to approximately 7 using 1 M $HCl_{(aq)}$, and the suspensions were dialyzed against deionized water (MWCO 100 Da) for at least 24 hours to remove salt and hydrolysis byproducts. Dialysate was changed at least 3 times. The hydrolyzed particles and polymers were then flash-frozen in liquid nitrogen and lyophilized prior to analysis with FTIR.

Neutron Scattering: Small angle neutron scattering SANS experiments were carried out on the NG7 30 m SANS instrument at the NIST Center for Neutron Research (NCNR) in Gaithersburg, MD. Neutrons of wavelength $\lambda = 6$ Å with a distribution of $\Delta\lambda/\lambda = 10$ % were incident on samples held in quartz cells. Three different sample to detector distances were used to give an overall q range of $0.0038\ Å^{-1} < q < 0.37\ Å^{-1}$, where $q = (4\pi/\lambda)\sin(\theta/2)$ is the magnitude of the scattering vector. Sample scattering was corrected for background and empty cell scattering, and the sensitivities of individual detector elements were normalized. The corrected data sets were circularly averaged and placed on an absolute scale using software supplied by the NCNR.[25]

USANS experiments were carried out on the BT5 perfect crystal diffractometer (PCD) at the NCNR using the same samples described above.

The overall q range was 3.8 x 10^{-5} $Å^{-1}$ < q < 0.002 $Å^{-1}$. All data were reduced and analyzed using software provided by the NCNR.[25] Here, only slit-smeared data are shown.

Samples for all neutron scattering experiments were prepared using D_2O as a solvent, thus the scattering length density of the solvent was 6.3 x 10^{-6} $Å^{-2}$. Particle densities were approximated using a weighted average of the neat monomer densities. Scattering length densities of the particles were calculated using the NCNR scattering length density calculator[26] with atomic scattering lengths obtained from V.F. Sears.[27]

Transmission Electron Microscopy TEM Imaging: TEM images were acquired on a Philips CM300FEG TEM (C_s = 1.2 mm) operated at 300 kV using a 10.8 mrad objective aperture semiangle. Samples were drop-mounted onto silicon-supported 25 nm thermal SiO_2 membranes (Dune Sciences NG01-011A) and allowed to dry in air for 24 hours before imaging. Samples were imaged using a Gatan GIF-200 in energy filtered mode using a 10 eV acceptance slit. To increase signal to noise ratios, the images were constructed from a series of 100, 0.5 second exposures, which were then aligned and summed to produce the final image.

Fourier Transform Infrared Spectroscopy: FTIR was used to determine the effects of hydrolysis on the functional groups present within the nanoparticles (Smith's Detection IlluminatIR FTIR Microscope). After lyophilization, hydrolyzed and non-hydrolyzed samples were resuspended in deionized water by sonicating in an ultrasonication bath for one hour. Particle and polymer suspensions were

then decanted onto a gold-plated microscope slide and allowed to dry at ambient conditions under a chemical hood. FTIR spectra were then collected from the resultant polymer and particle films. All experiments were conducted on a diamond attenuated total reflectance objective microscope accessory. Reported spectra are the average of 128 scans.

^{19}F-NMR Spectroscopy: ^{19}F spectra were acquired on a Bruker DRX 400 MHz NMR equipped with a QNP probe at The University of Kansas. The samples were suspended in D_2O and the spectrometer was locked to this solvent during the experiments. All samples were recorded with a sweep width of 99 ppm, a transmitter offset of -80 ppm and a 1 second delay. Spectra were collected with 16 scans on the particles synthesized with the 1H,H-perfluoro-n-octyl acrylate monomer and 64 scans were used for the particles synthesized using the 2-(allyl)hexafluoroisopropanol monomer.

III. Results

Small Angle Neutron Scattering: Fluorinated nanoparticles were prepared using a method similar to one described previously.[23] After purification, samples were suspended in D_2O and analyzed using SANS and USANS at several different concentrations. The scattering length density values for particles prepared with each of the fluorinated monomers are given in Table 1. Non-linear least-squares model fitting was performed using Schulz-distributed spheres of uniform scattering length density. The normalized Schulz distribution is given by Equation 1:

$$f(R) = \frac{(z+1)^{(z+1)}}{R_{avg}\Gamma(z+1)} x^z \exp\left[-(z+1)x\right] \qquad (1)$$

where R_{avg} is the mean radius of the particles, and x = R/R_{avg}, z is a function of the polydispersity, $p = \sigma/R_{avg}$, and $z = 1/p^2 - 1$, σ is the standard deviation of the distribution, and $\Gamma(z+1)$ is the gamma function. For a typical SANS experiment, the SANS intensity is given by Equation 2:

$$I(q) = \left(\frac{\Phi}{V_p}\right)\Delta\rho^2 P(q) S(q) + b \qquad (2)$$

where φ is the particle volume fraction, V_p is the particle volume, $\Delta\rho$ is the difference between the scattering length density of the particles and the scattering length density of the solvent (ρ_p - ρ_s), and b is the incoherent background scattering intensity. The function *P(q)* is the intraparticle form factor averaged over the Schulz distribution, and *S(q)* is the interparticle interference factor, which is equal to 1 in the case of non-interacting particles. The particles were confirmed to be non-interacting by measuring at several dilutions. Combining this equation with the normalized Schulz distribution yields Equation 3:

$$I(q) = \left(\frac{4\pi}{3}\right)^2\left(\frac{\phi}{\langle V\rangle}\right)\Delta\rho^2 \int_0^\infty f(R) R^6 F^2(qR)\, dR \qquad (3)$$

where, $\langle V\rangle$ is the average volume of a particle. The function *F* is the scattering amplitude of a sphere, and is given by Equation 4:

$$F(x) = \frac{\left[\sin(x) - x\cos(x)\right]}{x^3} \qquad (4)$$

The average volume, $\langle V \rangle$, is calculated using the 3rd moment of *R* and is given by Equation 5.

$$\langle V \rangle = \frac{4\pi}{3} \langle R_{avg} \rangle^3 \frac{(\xi+3)(\xi+2)}{(\xi+1)^2} \qquad (5)$$

For the particles prepared using the 1H,1H-perfluoro-n-octyl acrylate monomer, the USANS data were initially fit to obtain the size and polydispersity of the particles. For the smaller concentrations (concentrations less than 1 mg/mL), the polydispersity was held at the value calculated from the most concentrated sample. The SANS data were also fit using the parameters calculated from the USANS data, although the background and the volume fraction parameters were relaxed. The model was then fit to both the USANS and the SANS data simultaneously to optimize the fit. The spectra are shown in Figure 2, and the model parameters are listed in Table 2. The particles are between 390.1 nm ± 4.4 nm and 413.1 nm ± 2.6 nm in diameter with a polydispersity of 0.52, showing only a slight variation with dilution. The discrepancies between the volume fractions calculated for the USANS and SANS data for each concentration could be due to small amounts of particle settling that occurred while the samples were waiting for analysis on the SANS instrument.

For the 2-(allyl)hexafluoroisopropanol monomer, only spectra obtained for concentrations of 1 mg/mL and 0.5 mg/mL were analyzed due to insufficient scattering at lower concentrations. Only the USANS spectra were used in the analysis of 2-(allyl)hexafluoroisopropanol because the expected particle size was within the range suitable for USANS measurements. The model was fit to each

data set individually, and then to both concentrations simultaneously while holding the polydispersity from the highest concentrated sample constant to minimize the degrees of freedom and to ensure a consistent fit with both data sets. In the spectra for the particles prepared with the 2-(allyl)hexafluoroisopropanol monomer, the q-range was not large enough to accurately determine the particle polydispersity, so the polydispersity was held at 0.5, which is close to the value obtained for the particles prepared with the 1H,H-perfluoro-n-octyl acrylate monomer. The spectra for these particles are shown in Figure 3, and the model parameters are listed in Table 3. The model fit yields an average particle size of 281.2 nm ± 16.4 nm.

Transmission Electron Microscopy: The sizes of the fluorinated nanoparticles were further corroborated by the TEM images (Figure 4), which show particles prepared with the1H,H-perfluoro-n-octyl acrylate monomer (Panel A) that are less than 400 nm in diameter. Panel B shows particles prepared with the 2-(allyl)hexafluoroisopropanol monomer that are less than 500 nm in diameter. The observed particle sizes corroborated the neutron scattering data which suggested that the particles could potentially accumulate via the EPR effect.[17]

Fourier Transform Infrared Spectroscopy: Nanoparticles were analyzed using FTIR to determine the suitability of the particles for chemical modification and conjugation strategies. Analogous polymers prepared without the (1,5-N-vinylformamido) ethyl ether crosslinker or the PVP surfactant were also analyzed as a comparison. The ability to hydrolyze the amide to an amine could enable

one to conjugate a carboxyl terminated targeting ligand to the particles or polymers to facilitate active targeting of pathological tissue. This can be done with simple chemistry that is well described in the literature.[28, 29]

Particles prepared using the 1H,H-perfluoro-n-octyl acrylate monomer (Figure 5, Panel A) showed evidence of hydrolysis of both the formamide group and of the perfluorinated ester, as expected. Hydrolyzed particles showed a strong peak at 3326 cm^{-1}, which is within the hydrogen bonded OH region (3300 – 2500 cm^{-1}) and the primary aliphatic amine region (3450 – 3250 cm^{-1}). The emergence of the OH frequency was due to the hydrolysis of the perfluorinated acrylate (1H,H-perfluoro-n-octyl acrylate), which was hydrolyzed to a carboxylic acid. Although the presence of an amine after hydrolysis suggests that the particles can be bound to a targeting ligand using simple chemistry, the fact that the fluorinated ester was hydrolyzed indicates that particles prepared with the 1H,H-perfluoro-n-octyl acrylate monomer would not be suitable for use as an active targeting agent if conversion to the primary amine is a necessary reaction step.

The non-hydrolyzed particles prepared with the 1H,H-perfluoro-n-octyl acrylate showed a peak at 1753 cm^{-1} suggesting a carbonyl ester (1750 – 1725 cm^{-1}) and an amide I carbonyl peak (1670 – 1650 cm^{-1}), both of which were absent in the hydrolyzed particles' spectrum. The hydrolyzed particles also showed an N-H deformation peak at 1548 cm^{-1}, which is near the typical region (1650 – 1580 cm^{-1}) but was likely shifted to higher frequency due to hydrogen

bonding. This would indicate the presence of an amine. Representative structures of the non-hydrolyzed and hydrolyzed particles are shown in Figure 6.

The analogous polymer samples (Figure 5, Panel B) synthesized with the 1H,H-perfluoro-n-octyl acrylate monomer showed much evidence of hydrolysis. The hydrolyzed polymer spectrum showed a broad peak around 3300 cm^{-1}, which is indicative of both OH stretching (3300 – 2500 cm^{-1}) and primary amines (3450 – 3250 cm^{-1}). The non-hydrolyzed spectrum showed small peaks at 1749 cm^{-1} and 1669 cm^{-1}, both of which were absent in the hydrolyzed spectrum and indicated the presence of a carbonyl ester (1750 – 1725 cm^{-1}) and an amide I (carbonyl) peak (1670 – 1650 cm^{-1}), respectively. Additionally, two peaks at 1196 cm^{-1} and 1140 cm^{-1} were present in the non-hydrolyzed spectrum, and indicated the presence of an ester C-O stretch. These peaks were very obviously absent in the hydrolyzed spectrum, which suggested the hydrolysis of the fluorinated ester group.

Nanoparticles prepared using the 2-(allyl)hexafluoroisopropanol monomer (Figure 5, Panel C) qualitatively suggested hydrolysis of the formamide group on the N-vinylformamide monomer and the (1,5-N-vinylformamido) ethyl ether crosslinker. The non-hydrolyzed spectrum showed a peak at 3401 cm^{-1}, which is within the OH stretch region (3300 – 2500 cm^{-1}). Unfortunately, this overlapped with the primary amine region (3450 – 3250 cm^{-1}), making it difficult to distinguish the two. The hydrolyzed particles showed a broad peak at 3378 cm^{-1}. Because this frequency is shifted toward the primary amine region and is at higher intensity, it stands to reason that this peak was due to influence from both the

hydroxyl group on the 2-(allyl)hexafluoroisopropanol monomer and the primary amine from the hydrolyzed formamide groups. Additionally, both spectra showed peaks at 1648 cm^{-1}, which suggested the presence of a hydrogen-bonded carbonyl group. This is most likely from the formamide group (amide I), which was present in the non-hydrolyzed particles and was likely present within the hydrolyzed particles to some degree, possibly buried within the particles where they might be sterically shielded from hydrolysis. The high intensity of this peak is not observed in the linear hydrolyzed polymer, which further suggested that the crosslinking may have buried some of the formamide groups within the particles. The presence of an amine peak after hydrolysis suggested that these particles could be successfully conjugated with a carboxyl terminated targeting ligand, for example. Representative structures of the hydrolyzed and non-hydrolyzed particles are shown in Figure 6.

The spectra for the analogous polymer samples (Figure 5, Panel D) show evidence of formamide hydrolysis. Similar to the respective particles, both the hydrolyzed and non-hydrolyzed polymers showed peaks in the OH stretch region (3300 – 2500 cm^{-1}), which was expected from to the 2-(allyl)hexafluoroisopropanol monomer. This region overlaps with the primary aliphatic amine region (3450 – 3250 cm^{-1}) and is more intense for the hydrolyzed polymer, suggesting that this peak is influenced by both the hydroxyl group and the primary amine. Additional evidence for hydrolysis was the decrease in the intensity of the carbonyl peak (1650 cm^{-1}), which was likely shifted to a higher frequency in both spectra due to hydrogen bonding. The lower intensity of this

peak in the hydrolyzed sample could indicate the loss of the formamide group, which would be expected. The fact that this peak did not diminish in intensity in the particles could be due to the crosslinking, which might bury formamide groups within the particles, again rendering them sterically isolated from hydrolysis.

^{19}F NMR Spectroscopy: Nanoparticle samples were analyzed using ^{19}F-NMR to determine their potential as ^{19}F-MRI contrast agents (Figure 7). Particles prepared with the 1H,H-perfluoro-n-octyl acrylate monomer showed a peak between -83 ppm and -84 ppm (Figure 7, Panel A). This peak corresponds to the CF_2 group closest to the oxygen atom. Additionally, the spectrum shows an out-of-phase signal near -121 ppm (inset), which is from the perfluorinated region ($-CF_2CF_2-$) of the pendant group. Particles prepared with the 2-(allyl)hexafluoroisopropanol monomer showed a peak around -76 ppm (Figure 7, Panel B). This peak is similar to the CF_2 peak from the 1H,H-perfluoro-n-octyl acrylate particles because both have the same proximity to a nearby oxygen atom. Both particles exhibited fairly narrow widths in their ^{19}F-NMR spectra, suggesting that some fluorinated groups are well solvated with a degree of mobility. The particles would produce a ^{19}F-MRI signal and therefore hold potential for use as a ^{19}F-MRI contrast agent.[1]

IV. Discussion

Current studies in the area of ^{19}F MRI contrast agents have validated the premise of developing colloidally stable, fluorinated contrast agents using

nanoemulsions that contain a liquid perfluorocarbon phase. These studies have investigated fluorinated liquids such as perfluoro-15-crown-5-ether and perfluorooctyl bromide, which were emulsified into an aqueous phase using an appropriate biocompatible surfactant.[5, 7, 14, 30] Other studies have created novel fluorinated amphiphilic block copolymers that formed micelles in water, typically using a living free radical polymerization method.[1, 8, 9, 31] In a previous study, the idea of synthesizing fluorinated nanoparticles using a single step, free radical polymerization technique was validated.[23] In this study, fluorinated nanoparticles were prepared using a free radical polymerization method that contained a hydrophilic monomer, a hydrophilic crosslinker, and one of two fluorinated monomers. Future studies will continue to optimize the reaction method to produce particles of smaller size by better controlling the reaction rate to encourage the formation of smaller molecular weight polymers, which should lead to smaller particles. After synthesis, the particles were evaluated for their suitability as a ^{19}F MRI contrast agent that can be targeted to specific pathological sites (e.g. tumors, atherosclerosis) using either active or passive targeting strategies.

A potential passive targeting strategy that has been investigated as a means to deliver antineoplastic agents to tumors exploits the anatomical and physiological abnormalities of tumor vasculature.[18] Typically, the blood vessels in tumor tissue are tortuous, poorly organized and contain numerous pores due to large gap junctions between endothelial cells, which can compromise lymphatic drainage.[17-21] These anatomical aberrations can cause extensive

leakage of macromolecular agents and small nanoparticles from the capillaries into the tumor interstitium, where they can accumulate.[18] This phenomenon is called the enhanced permeability and retention effect (EPR effect), and has been studied using macromolecular therapeutic agents.[32, 33] It has also been observed with polymeric nanoparticles that are several hundred nanometers in diameter.[34] Neutron scattering measurements and TEM images indicated that the particles prepared in this study are between approximately 200 nm and 400 nm in diameter, suggesting that they might be a bit large for use in passive targeting applications.

Additionally, active targeting strategies using ligands that specifically bind selected tumor targets may amplify the specificity of nanoparticles.[16, 17] For example, amine-functionalized nanoparticles will react with ligands terminated with succinimide esters or isothiocyanates.[35] Carboxylated nanoparticles or ligands can be made reactive toward amine-terminated moieties using 1-ethyl-3-(dimethylaminopropyl)carbodiimide (EDC) and either N-hydroxysuccinimide (NHS) or N-hydroxysulfosuccinimide (sulfo-NHS) to form an amine-reactive succinimide ester.[35] FTIR spectra suggested that formamide groups on the surface of nanoparticles and linear polymers prepared in this study using the 2-(allyl)hexafluoroisopropanol fluorinated monomer can be hydrolyzed at high pH to liberate amine groups, yielding reactive sites for ligand conjugation to facilitate active targeting strategies. Future studies will evaluate the reactivity of the amines and the amides to determine the most effective conjugation strategy for active targeting.

In addition to tumor imaging, another potential clinical application for nanoparticle-based MRI contrast agents is atherosclerosis imaging. This technique could prove useful in identifying patients at high-risk for myocardial infarction who have not been identified by routine clinical evaluation, and may also be useful in characterizing the vulnerability of atheroma present in high-risk areas of the coronary vasculature.[37] As an active targeting technique, nanoparticles could be conjugated with a ligand that would facilitate binding to proinflammatory adhesion molecules expressed during atherogenesis. Possible targets include intercellular cell-adhesion molecule-1 (ICAM-1) and vascular cell-adhesion molecule-1 (VCAM-1), both of which are expressed on the endothelium around atherosclerotic lesions.[37-39] Studies have also developed paramagnetic MRI contrast agents that actively target thrombus.[40, 41] Paramagnetic contrast agents have also been designed to target integrins associated with angiogenesis because of the high vascularity of atherosclerotic lesions compared to normal vessel tissues.[42] Another study targeted macrophages, which are key effector inflammatory cells in atherosclerosis.[43] Analogous methods of targeting atheroma using ultrasound contrast agents have also been demonstrated.[39]

Although the linear polymers synthesized in this study were used only as a control, they could have diagnostic applications that should be evaluated in the future. For example, linear polymers synthesized from the 2-(allyl)hexafluoroisopropanol and N-vinylformamide monomers were soluble in water, but presumably formed micelles approximately 200 nm in diameter, as estimated by dynamic light scattering measurements. Ultimately, the water

solubility and narrow ^{19}F MRI spectra of this polymer may facilitate translation into animal models.

V. Conclusions

A novel synthetic approach for obtaining functional fluorinated nanoparticles was explored. The results of this study suggested that fluorinated nanoparticles prepared using a simple free radical polymerization technique would produce a sufficient magnetic resonance signal for ^{19}F-MRI contrast enhancement. Nanoparticles may be useful for passive targeting strategies that rely on phenomena such as the enhanced permeability and retention (EPR) effect, as well as active targeting strategies that rely on targeting ligands to amplify nanoparticle uptake into pathological tissue, such as tumor tissue or atherosclerotic lesions. Nanoparticles or polymers prepared using the 2-(allyl)hexafluoroisopropanol fluorinated monomer may be hydrolyzed to liberate free amines for additional conjugation schemes while maintaining the integrity of the fluorinated moiety. Future studies will examine the uptake of ligand-conjugated nanoparticles in *in vitro* cell culture, as well as the *in vivo* efficacy of fluorinated nanoparticles as ^{19}F-MRI contrast media.

Acknowledgement

The authors graciously acknowledge the Student Temporary Employment Program (STEP) at NIST, as well as Dr. Greg Gillen for his mentorship. They would also like to acknowledge funding from the Madison and Lila Self Graduate

Fellowship at The University of Kansas, as well as additional funding from the Coulter Foundation, the Higuchi Biosciences Center, and the American Heart Association. In addition, they would like to acknowledge funding from the NIH (R03 AR054035 and P20 RR016443) and the NSF (CHE 0719464 and DMR-0944772). The authors also acknowledge The University of Oregon's NSF IGERT Fellowship Program under grant number DGE-0549503. Finally, the authors would like to thank Sarah Neuenswander at the KU Nuclear Magnetic Resonance Laboratory for her assistance with data acquisition, and Loren Schieber at The University of Kansas for valuable discussions.

Tables

Table 1: Scattering Length Densities of Fluorinated Nanoparticles

Monomer	Estimated Particle Density (g/cm^3)	Scattering Length Density ($Å^{-2}$)
1H,1H-perfluoro-n-octyl acrylate	1.30	3.00×10^{-6}
2-Allyl hexafluoroisopropanol	1.15	2.73×10^{-6}

Table 2: Model parameters for nanoparticles prepared with 1H,1H-perfluoro-n-octyl acrylate monomer

	1 mg/mL		0.5 mg/mL		0.2 mg/mL		0.1 mg/mL	
Parameter	SANS	USANS	SANS	USANS	SANS	USANS	SANS	USANS
Volume Fraction	$2.99 \times 10^{-3} \pm 2.8 \times 10^{-5}$	$1.32 \times 10^{-3} \pm 1.4 \times 10^{-5}$	$1.30 \times 10^{-3} \pm 1.3 \times 10^{-5}$	$3.54 \times 10^{-4} \pm 4.1 \times 10^{-6}$	$5.92 \times 10^{-4} \pm 6.5 \times 10^{-6}$	$1.41 \times 10^{-4} \pm 1.9 \times 10^{-6}$	$2.88 \times 10^{-4} \pm 4.8 \times 10^{-6}$	$6.03 \times 10^{-5} \pm 1.1 \times 10^{-6}$
Mean Diameter (nm)	413.1 ± 2.6		410.6 ± 2.8		399.1 ± 3.0		390.1 ± 4.4	
Polydispersity	0.522		0.522		0.522		0.522	
Background (cm^{-1} sr^{-1})	0.071		0.057		0.056		0.059	

Error is equal to 1 standard deviation of the fitted value. Values without reported error were held exact during model convergence.

Table 3: Model parameters for nanoparticles prepared with 2-allyl hexafluoroisopropanol monomer

Parameter	1 mg/mL	0.5 mg/mL
Volume Fraction	$1.62 \times 10^{-3} \pm 1.5 \times 10^{-4}$	$6.56 \times 10^{-4} \pm 6.2 \times 10^{-5}$
Mean Diameter (nm)	281.2 ± 16.4	
Polydispersity	0.5	
Background (cm^{-1} sr^{-1})	0.218	

Error is equal to 1 standard deviation of the fitted value. Values without reported error were held exact during model convergence.

Figure 1:

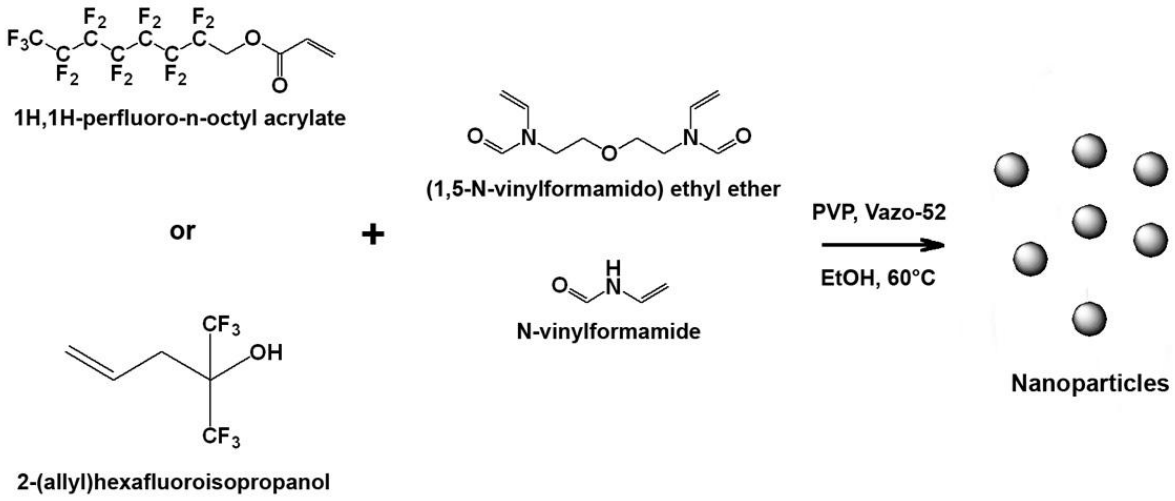

Figure 1:
Diagram of the reaction scheme. For each batch, one of the fluorinated monomers was reacted with (1,5-N-vinylformamido) ethyl ether and N-vinylformamide to generate nanoparticles. The reaction was carried out in ethanol at 60°C using Vazo-52 as an initiator and polyvinylpyrrolidone (PVP) as a surfactant. For the analogous polymers, the same reaction scheme was used, but without the addition of the (1,5-N-vinylformamido) ethyl ether crosslinker or the PVP surfactant.

Figure 2:

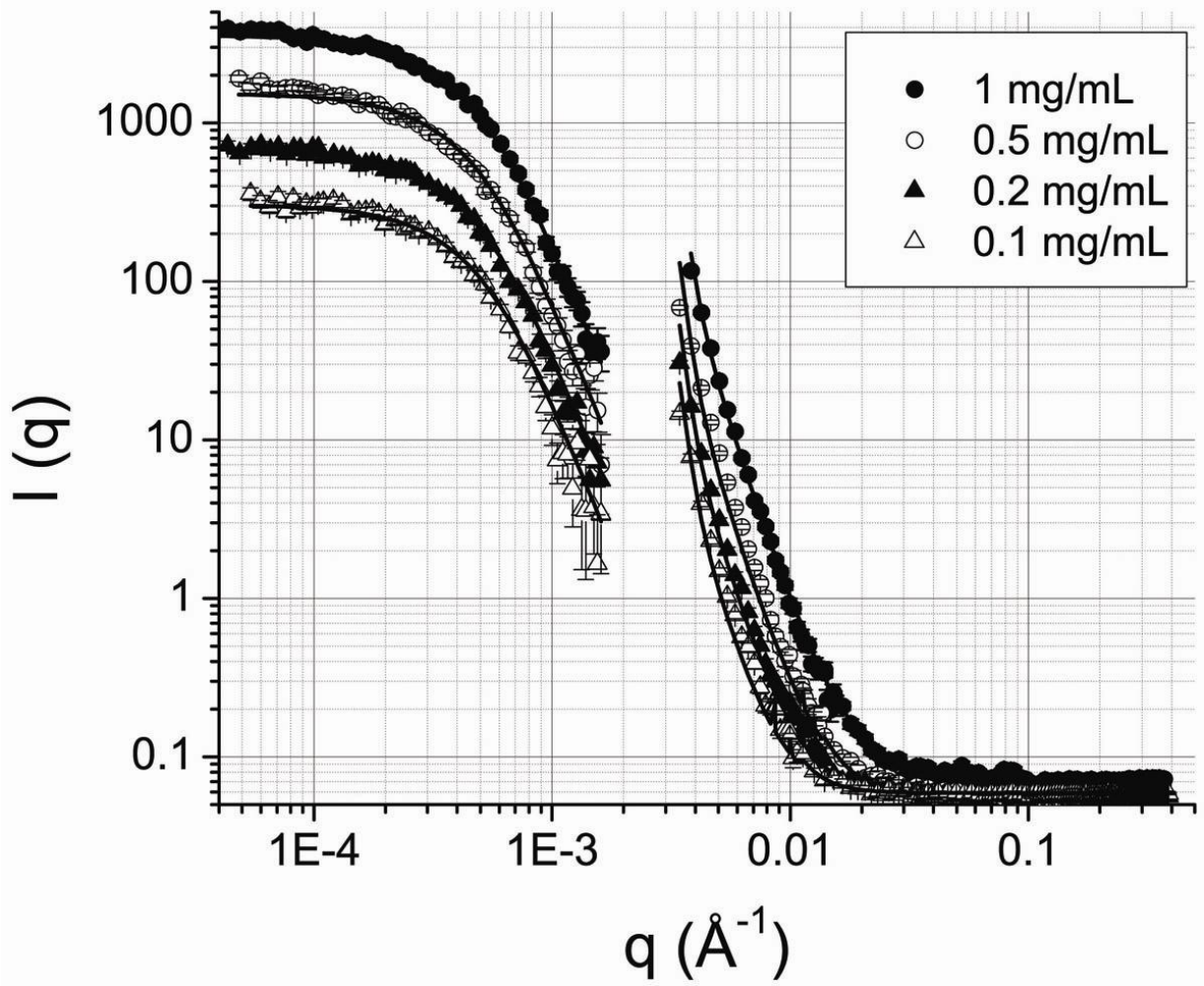

Figure 2:
USANS and SANS spectra of particles prepared with 1H,1H-perfluoro-n-octyl acrylate monomer. Particles were dispersed in D_2O without surfactant at various concentrations. Data were fit using a Schulz sphere analytical model. The model suggested that the particles are between 390 and 414 nm in diameter with a polydispersity of approximately 0.52.

Figure 3:

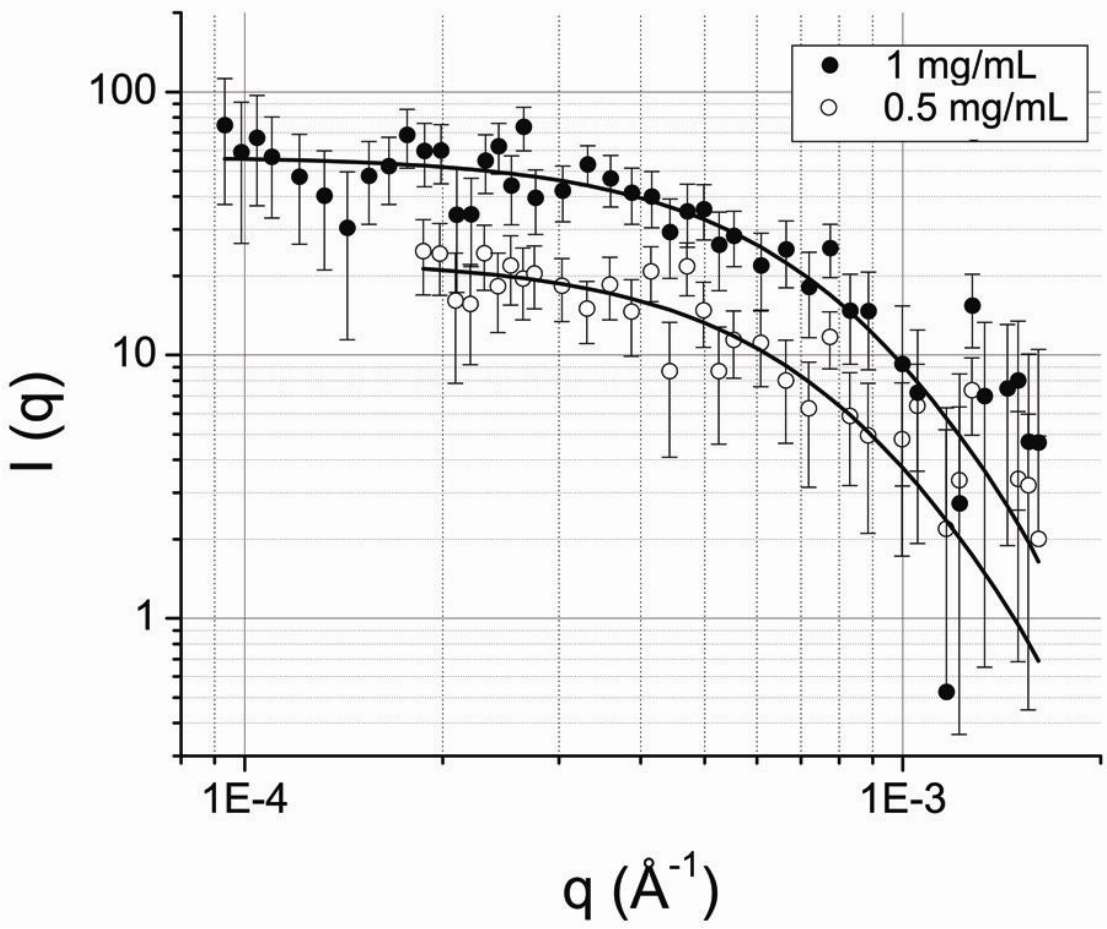

Figure 3:
USANS spectra of particles prepared with 2-(allyl)hexafluoroisopropanol monomer. Particles were dispersed in D_2O without surfactant at concentrations of 1 mg/mL and 0.5 mg/mL. Data were fit using a Schulz sphere analytical model with the result that the particles are 282 nm ± 16 nm in diameter. The polydispersity was held to 0.5 due to the limited q-range.

Figure 4:

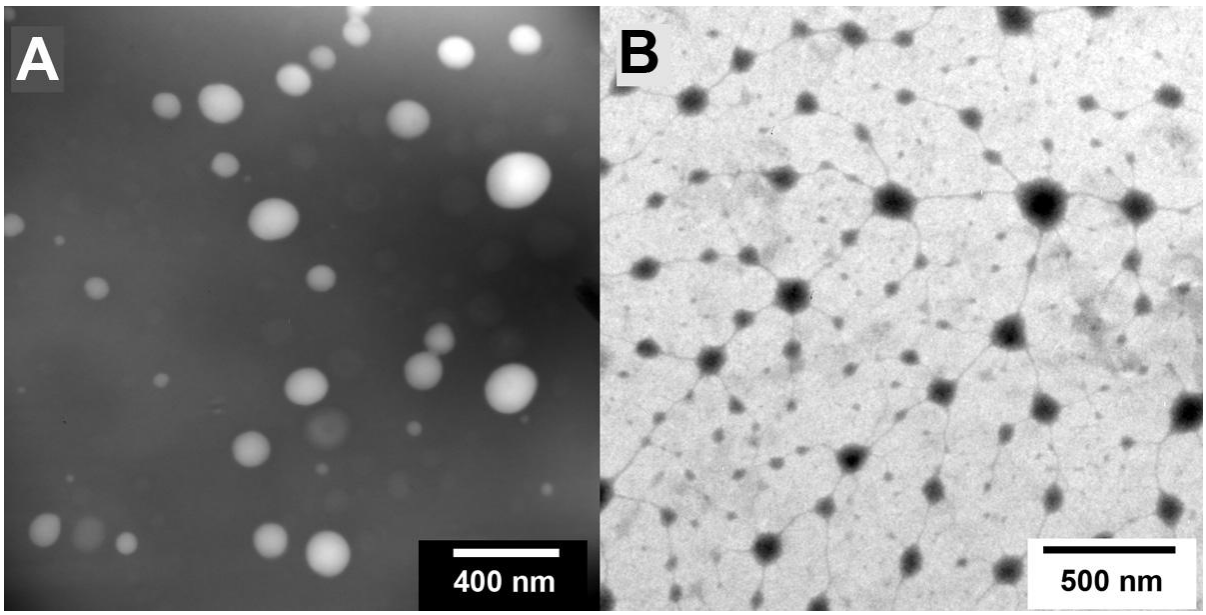

Figure 4:
TEM Image of particles prepared with 1H,H-perfluoro-n-octyl acrylate monomer (A) and 2-(allyl)hexafluoroisopropanol monomer (B).

Figure 5:

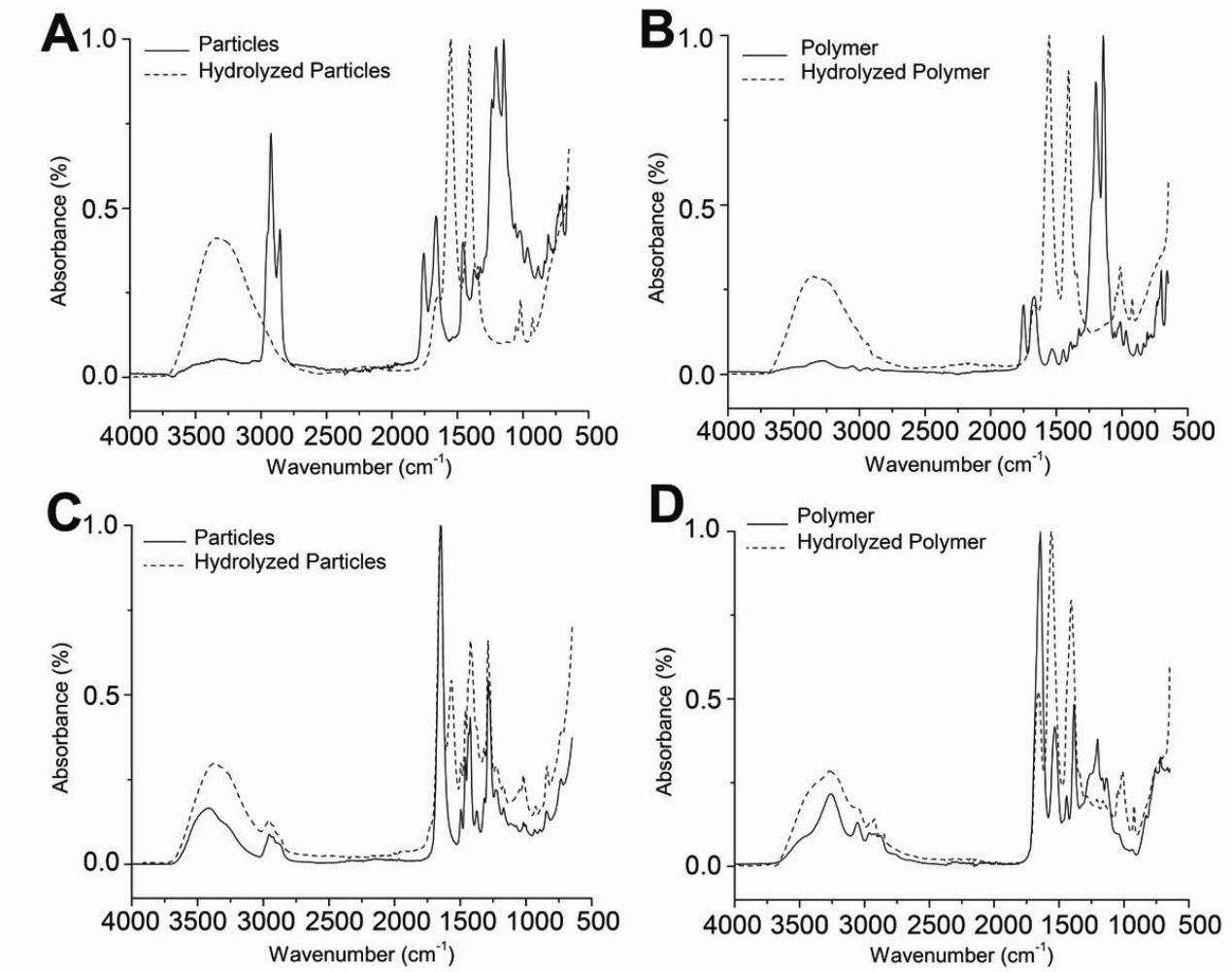

Figure 5:
FTIR spectra of fluorinated nanoparticles. (A) particles and (B) polymer prepared with 1H,1H-perfluoro-n-octyl acrylate monomer. (C) particles and (D) polymer prepared with the 2-(allyl)hexafluoroisopropanol monomer. All solutions were allowed to evaporate prior to analysis of the resultant nanoparticle or polymer film.

Figure 6:

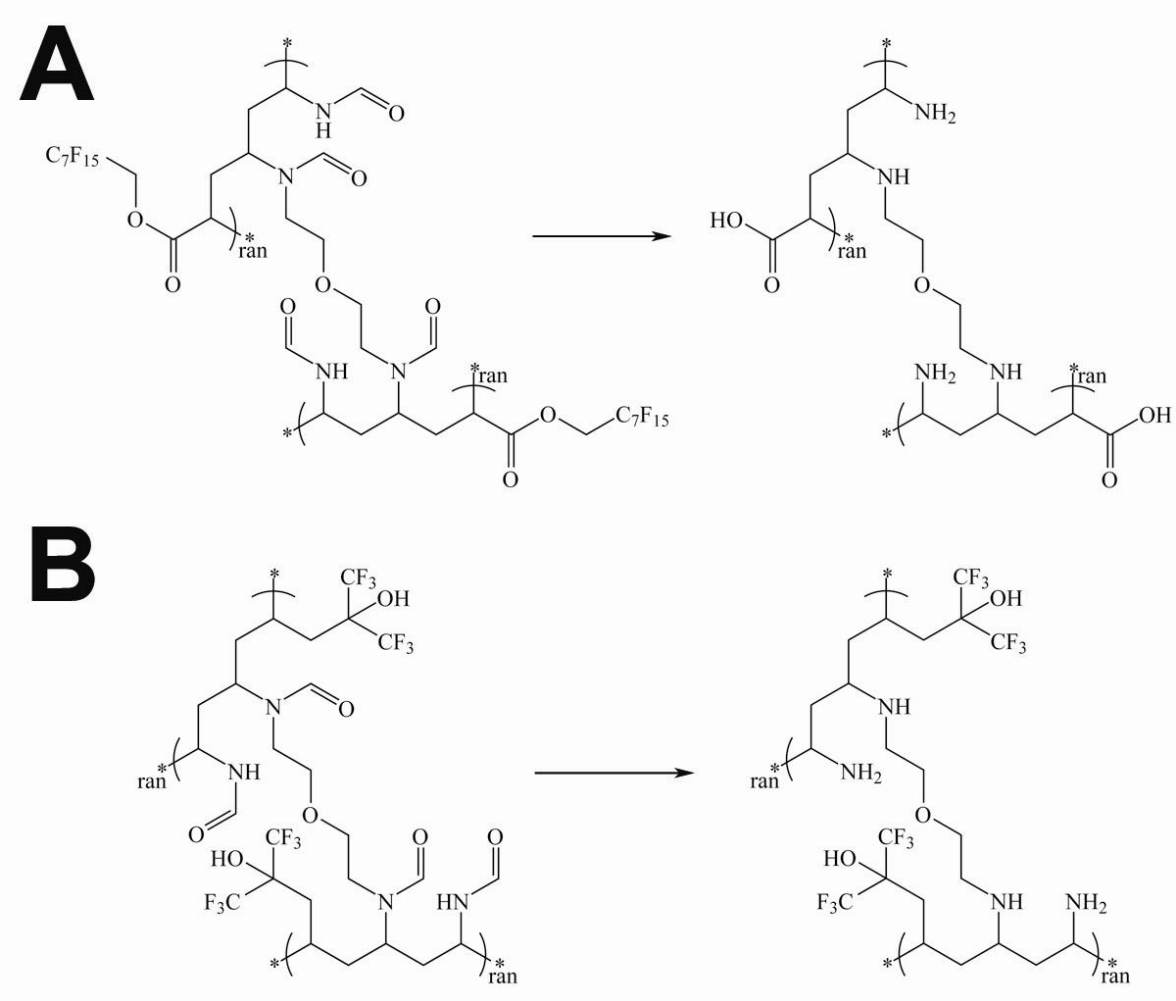

Figure 6:
Representative chemical structures of non-hydrolyzed and hydrolyzed particles prepared using the different monomers. (A) Hydrolysis of particles prepared using the 1H,1H-perfluoro-n-octyl acrylate monomer, where amide groups were hydrolyzed to their corresponding amines, and the fluorinated ester was also cleaved. (B) Hydrolysis of particles prepared using the 2-(allyl)hexafluoroisopropanol monomer, where the amide groups were converted to primary and secondary amines, while the fluorinated regions remained intact.

Figure 7:

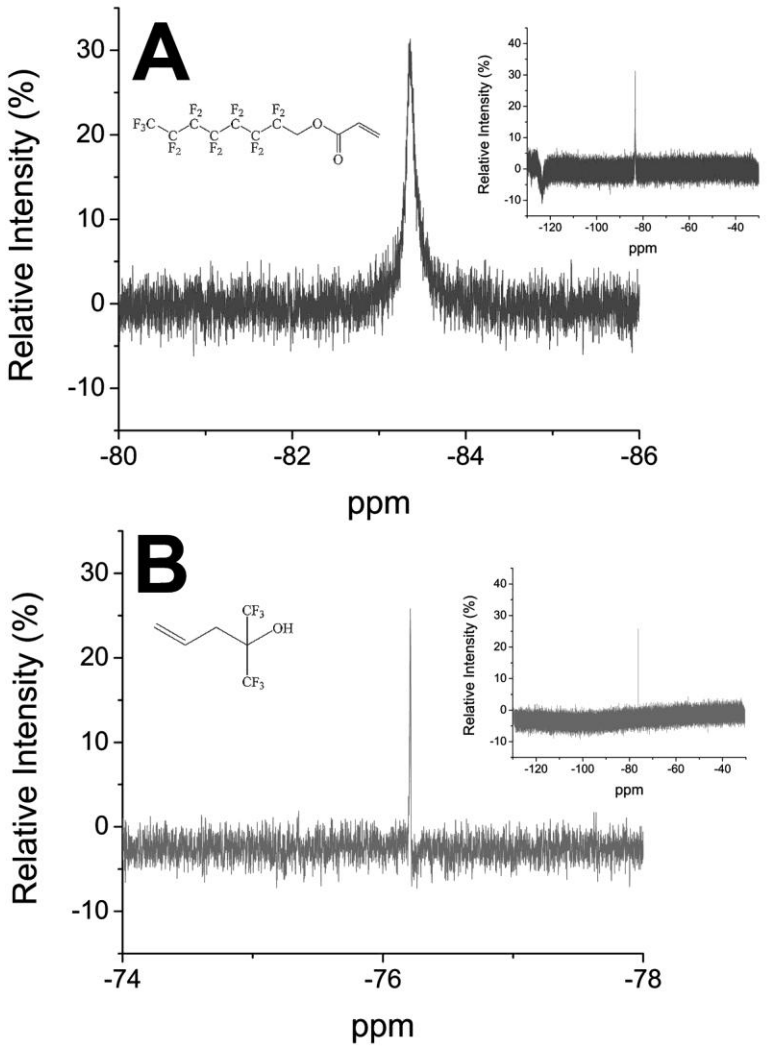

Figure 7:
^{19}F-NMR spectra of fluorinated nanoparticles. (A) The spectrum for nanoparticles prepared using the 1H,1H-perfluoro-n-octyl acrylate monomer shows a broad peak at -83.35 ppm. (B) The spectrum for nanoparticles prepared using the 2-(allyl)hexafluoroisopropanol monomer shows a sharp peak at -76.21 ppm. Insets show the spectra for the entire sweep width.

References

1. Du, W. J.; Nystrom, A. M.; Zhang, L.; Powell, K. T.; Li, Y. L.; Cheng, C.; Wickline, S. A.; Wooley, K. L., Amphiphilic Hyperbranched Fluoropolymers as Nanoscopic F-19 Magnetic Resonance Imaging Agent Assemblies. *Biomacromolecules* **2008,** 9, (10), 2826-2833.
2. Huang, M.; Huang, Z. L.; Bilgen, M.; Berkland, C., Magnetic resonance imaging of contrast-enhanced polyelectrolyte complexes. *Nanomedicine* **2008,** 4, (1), 30-40.
3. Lauffer, R. B., Paramagnetic Metal-Complexes as Water Proton Relaxation Agents for Nmr Imaging - Theory and Design. *Chemical Reviews* **1987,** 87, (5), 901-927.
4. Caravan, P.; Ellison, J. J.; McMurry, T. J.; Lauffer, R. B., Gadolinium(III) chelates as MRI contrast agents: Structure, dynamics, and applications. *Chemical Reviews* **1999,** 99, (9), 2293-2352.
5. Buchanan, G. W.; Moudrakovski, I., F-19 magnetic resonance imaging using vesicles of sucrose octaoleate-F-104. *Journal of Fluorine Chemistry* **2008,** 129, (2), 137-138.
6. Duconge, F.; Pons, T.; Pestourie, C.; Herin, L.; Theze, B.; Gombert, K.; Mahler, B.; Hinnen, F.; Kuhnast, B.; Dolle, F.; Dubertret, B.; Tavitian, B., Fluorine-18-labeled phospholipid quantum dot micelles for in vivo multimodal imaging from whole body to cellular scales. *Bioconjugate Chemistry* **2008,** 19, (9), 1921-1926.
7. Fan, X. B.; River, J. N.; Muresan, A. S.; Popescu, C.; Zamora, M.; Culp, R. M.; Karczmar, G. S., MRI of perfluorocarbon emulsion kinetics in rodent mammary tumours. *Physics in Medicine and Biology* **2006,** 51, (2), 211-220.
8. Janjic, J. M.; Srinivas, M.; Kadayakkara, D. K. K.; Ahrens, E. T., Self-delivering nanoemulsions for dual fluorine-19 MRI and fluorescence detection. *Journal of the American Chemical Society* **2008,** 130, (9), 2832-2841.
9. Peng, H.; Blakey, I.; Dargaville, B.; Rasoul, F.; Rose, S.; Whittaker, A. K., Synthesis and Evaluation of Partly Fluorinated Block Copolymers as MRI Imaging Agents. *Biomacromolecules* **2009,** 10, (2), 374-381.
10. Srinivas, M.; Morel, P. A.; Ernst, L. A.; Laidlaw, D. H.; Ahrens, E. T., Fluorine-19 MRI for visualization and quantification of cell migration in a diabetes model. *Magn Reson Med* **2007,** 58, (4), 725-34.
11. Krafft, M. P., Fluorocarbons and fluorinated amphiphiles in drug delivery and biomedical research. *Advanced Drug Delivery Reviews* **2001,** 47, (2-3), 209-228.
12. Riess, J. G., Fluorous micro- and nanophases with a biomedical perspective. *Tetrahedron* **2002,** 58, (20), 4113-4131.
13. Riess, J. G., Blood substitutes and other potential biomedical applications of fluorinated colloids. *Journal of Fluorine Chemistry* **2002,** 114, (2), 119-126.

14. Flogel, U.; Ding, Z.; Hardung, H.; Jander, S.; Reichmann, G.; Jacoby, C.; Schubert, R.; Schrader, J., In vivo monitoring of inflammation after cardiac and cerebral ischemia by fluorine magnetic resonance imaging. *Circulation* **2008,** 118, (2), 140-8.
15. Schwarz, R.; Schuurmans, M.; Seelig, J.; Kunnecke, B., F-19-MRI of perfluorononane as a novel contrast modality for gastrointestinal imaging. *Magnetic Resonance in Medicine* **1999,** 41, (1), 80-86.
16. Brannon-Peppas, L.; Blanchette, J. O., Nanoparticle and targeted systems for cancer therapy. *Advanced Drug Delivery Reviews* **2004,** 56, (11), 1649-1659.
17. Cho, K. J.; Wang, X.; Nie, S. M.; Chen, Z.; Shin, D. M., Therapeutic nanoparticles for drug delivery in cancer. *Clinical Cancer Research* **2008,** 14, (5), 1310-1316.
18. Iyer, A. K.; Khaled, G.; Fang, J.; Maeda, H., Exploiting the enhanced permeability and retention effect for tumor targeting. *Drug Discovery Today* **2006,** 11, (17-18), 812-818.
19. Matsumura, Y.; Maeda, H., A New Concept for Macromolecular Therapeutics in Cancer-Chemotherapy - Mechanism of Tumoritropic Accumulation of Proteins and the Antitumor Agent Smancs. *Cancer Research* **1986,** 46, (12), 6387-6392.
20. Skinner, S. A.; Tutton, P. J. M.; Obrien, P. E., Microvascular Architecture of Experimental Colon Tumors in the Rat. *Cancer Research* **1990,** 50, (8), 2411-2417.
21. Suzuki, M.; Hori, K.; Abe, I.; Saito, S.; Sato, H., A New Approach to Cancer-Chemotherapy - Selective Enhancement of Tumor Blood-Flow with Angiotensin-Ii. *Journal of the National Cancer Institute* **1981,** 67, (3), 663-669.
22. Shi, L. J.; Berkland, C., pH-Triggered dispersion of nanoparticle clusters. *Advanced Materials* **2006,** 18, (17), 2315-+.
23. Bailey, M. M.; Mahoney, C. M.; Dempah, K. E.; Davis, J. M.; Becker, M. L.; Khondee, S.; Munson, E. J.; Berkland, C., Fluorinated Copolymer Nanoparticles for Multimodal Imaging Applications. *Macromolecular Rapid Communications* **2010,** 31, (1), 87-92.
24. Shi, L. J.; Berkland, C., Acid-labile polyvinylamine micro- and nanogel capsules. *Macromolecules* **2007,** 40, (13), 4635-4643.
25. Kline, S. R., Reduction and analysis of SANS and USANS data using IGOR Pro. *Journal of Applied Crystallography* **2006,** 39, 895-900.
26. Munter, A. Scattering Length Density Calculator. http://www.ncnr.nist.gov/resources/sldcalc.html (1 November),
27. Sears, V. F., Neutron Scattering Lengths and Cross Sections. *Neutron News* **1992,** 3, (3), 29-37.
28. Chittasupho, C.; Xie, S. X.; Baoum, A.; Yakovleva, T.; Siahaan, T. J.; Berkland, C. J., ICAM-1 targeting of doxorubicin-loaded PLGA nanoparticles to lung epithelial cells. *Eur J Pharm Sci* **2009,** 37, (2), 141-50.
29. Devaraj, N. K.; Keliher, E. J.; Thurber, G. M.; Nahrendorf, M.; Weissleder, R., F-18 Labeled Nanoparticles for in Vivo PET-CT Imaging. *Bioconjugate Chemistry* **2009,** 20, (2), 397-401.

30. Partlow, K. C.; Chen, J.; Brant, J. A.; Neubauer, A. M.; Meyerrose, T. E.; Creer, M. H.; Nolta, J. A.; Caruthers, S. D.; Lanza, G. M.; Wickline, S. A., 19F magnetic resonance imaging for stem/progenitor cell tracking with multiple unique perfluorocarbon nanobeacons. *Faseb J* **2007,** 21, (8), 1647-54.
31. Matson, J. B.; Grubbs, R. H., Synthesis of fluorine-18 functionalized nanoparticles for, use as in vivo molecular imaging agents. *Journal of the American Chemical Society* **2008,** 130, (21), 6731-+.
32. Nakanishi, T.; Fukushima, S.; Okamoto, K.; Suzuki, M.; Matsumura, Y.; Yokoyama, M.; Okano, T.; Sakurai, Y.; Kataoka, K., Development of the polymer micelle carrier system for doxorubicin. *Journal of Controlled Release* **2001,** 74, (1-3), 295-302.
33. Satchi-Fainaro, R.; Puder, M.; Davies, J. W.; Tran, H. T.; Sampson, D. A.; Greene, A. K.; Corfas, G.; Folkman, J., Targeting angiogenesis with a conjugate of HPMA copolymer and TNP-470. *Nature Medicine* **2004,** 10, (3), 255-261.
34. Kim, J. H.; Kim, Y. S.; Park, K.; Lee, S.; Nam, H. Y.; Min, K. H.; Jo, H. G.; Park, J. H.; Choi, K.; Jeong, S. Y.; Park, R. W.; Kim, I. S.; Kim, K.; Kwon, I. C., Antitumor efficacy of cisplatin-loaded glycol chitosan nanoparticles in tumor-bearing mice. *Journal of Controlled Release* **2008,** 127, (1), 41-49.
35. McCarthy, J. R.; Weissleder, R., Multifunctional magnetic nanoparticles for targeted imaging and therapy. *Advanced Drug Delivery Reviews* **2008,** 60, (11), 1241-1251.
36. Hecker, J. G.; Berger, G. O.; Scarfo, K. A.; Zou, S. M.; Nantz, M. H., A flexible method for the conjugation of aminooxy ligands to preformed complexes of nucleic acids and lipids. *Chemmedchem* **2008,** 3, (9), 1356-1361.
37. Jaffer, F. A.; Libby, P.; Weissleder, R., Molecular and cellular imaging of atherosclerosis: emerging applications. *J Am Coll Cardiol* **2006,** 47, (7), 1328-38.
38. Anderson, M. E.; Siahaan, T. J., Mechanism of binding and internalization of ICAM-1-derived cyclic peptides by LFA-1 on the surface of T cells: a potential method for targeted drug delivery. *Pharm Res* **2003,** 20, (10), 1523-32.
39. Hamilton, A. J.; Huang, S. L.; Warnick, D.; Rabbat, M.; Kane, B.; Nagaraj, A.; Klegerman, M.; McPherson, D. D., Intravascular ultrasound molecular Imaging of atheroma components in vivo. *Journal of the American College of Cardiology* **2004,** 43, (3), 453-460.
40. Flacke, S.; Fischer, S.; Scott, M. J.; Fuhrhop, R. J.; Allen, J. S.; McLean, M.; Winter, P.; Sicard, G. A.; Gaffney, P. J.; Wickline, S. A.; Lanza, G. M., Novel MRI contrast agent for molecular imaging of fibrin: implications for detecting vulnerable plaques. *Circulation* **2001,** 104, (11), 1280-5.
41. Yu, X.; Song, S. K.; Chen, J.; Scott, M. J.; Fuhrhop, R. J.; Hall, C. S.; Gaffney, P. J.; Wickline, S. A.; Lanza, G. M., High-resolution MRI characterization of human thrombus using a novel fibrin-targeted paramagnetic nanoparticle contrast agent. *Magn Reson Med* **2000,** 44, (6), 867-72.
42. Winter, P. M.; Morawski, A. M.; Caruthers, S. D.; Fuhrhop, R. W.; Zhang, H.; Williams, T. A.; Allen, J. S.; Lacy, E. K.; Robertson, J. D.; Lanza, G. M.; Wickline, S. A., Molecular imaging of angiogenesis in early-stage atherosclerosis with alpha(v)beta3-integrin-targeted nanoparticles. *Circulation* **2003,** 108, (18), 2270-4.

43. Jaffer, F. A.; Libby, P.; Weissleder, R., Molecular Imaging of cardiovascular disease. *Circulation* **2007,** 116, (9), 1052-1061.